because the centre point of each of the pentagonal 'dimples' constitutes an infinitesimally narrow tunnel giving access to a central icosahedral cavity.

The topological concept of genus is most simply appreciated as a generalization of Euler's rule (Ball, 1959): if $F$, $V$ and $E$ are the numbers of faces, vertices and edges of the polyhedron then its surface is of genus $\frac{1}{2}(2+E-F-V)$. If the genus is zero the surface is simply connected, *i.e.* deformable into a sphere. For compound facetions the formula must be applied to the component polyhedra individually. A face of which the edges form $n$ distinct chains must be counted $n$ times, as must a vertex with $n$ distinct chains of edges in its vertex polygon.

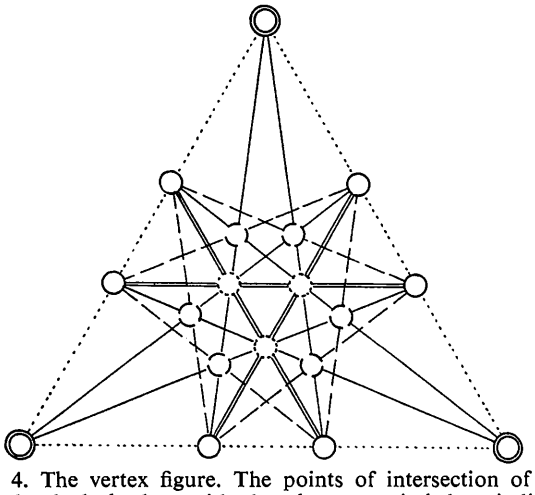

Fig. 4. The vertex figure. The points of intersection of the dodecahedral edges with the plane are circled to indicate the type of edge, as in Fig. 1. Also shown are the corresponding reciprocal lines, which form the edges in the face-plane of the icosahedron.

Thus it appears that 44 of the '59 icosahedra' (Coxeter *et al.*, 1938) have no reciprocals. In all of these it is impossible to describe the face by a polygon which satisfies rule 5, so that any attempt at reciprocation gives a figure with more than two faces meeting along some edges. It is interesting that of the dual pair of rules 4 and 5, 5 is trivial for facetted dodecahedra while 4 is intuitively obvious but in stellating the icosahedron it is 4 which is trivial while 5 is not obvious at all.

### References


BALL, W. W. R. (1959). *Mathematical Recreations and Essays*, 11th ed., revised by H. S. M. COXETER, p. 233. London: Macmillan.

COXETER, H. S. M. (1963). *Regular Polytopes*, 2nd ed., pp. 93–100. London: Macmillan.

COXETER, H. S. M., DU VAL, P., FLATHER, H. T. & PETRIE, J. F. (1938). *The Fifty-nine Icosahedra*. Univ. of Toronto Press.


*Acta Cryst.* (1974). A30, 552

# Interpretation of the 10Å Rotation Function of the Satellite Tobacco Necrosis Virus


BY PAUL J. LENTZ JR AND BROR STRANDBERG

*Wallenberg Laboratory, University of Uppsala, Uppsala, Sweden*


(*Received* 19 *February* 1974; *accepted* 18 *March* 1974)


The rotation function calculated with 10 Å three-dimensional data from monoclinic crystals of the satellite tobacco necrosis virus was fitted numerically to an icosahedral axis set. The r.m.s. angular deviation of the observed peak maxima from the calculated model axis set was 0·67° and the largest deviation was 1·4°. Thus, there is no significant deviation from icosahedral symmetry at 10 Å resolution. An investigation of the effects of the data inclusion limits and the radius of integration on the resolution of neighboring peaks in the rotation function showed that the best resolution was obtained by using only a thin shell of the highest-resolution data available and a radius of integration no larger than the estimated diameter of the virus protein subunit.


## Introduction

The crystallization of a virus, the tobacco mosaic virus, was first reported by Stanley (1935). Soon thereafter a number of small spherical plant viruses were crystallized and in 1944 X-ray diffraction patterns were obtained from dried crystals of a very small virus-like particle then called 'derivative' or 'protein' of the tobacco necrosis virus (TNV; Crowfoot & Schmidt, 1945). The particle was about one-third the molecular weight of TNV with which it was associated during infection and was thought to be a byproduct of infection rather than a separate virus. It is now recognized as the satellite tobacco necrosis virus (STNV) which, although antigenically unrelated to TNV, requires simultaneous co-infection by TNV in order to produce progeny (Kassanis & Nixon, 1961).

Crick & Watson (1956) proposed that the structural protein coat of small spherical viruses was made up of a number of identical subunits packed with cubic point symmetry to form the virus surface. This theory was formalized and extended by Caspar & Klug (1962)

who concluded that the icosahedral point group, 532, was much preferred for enclosing a volume with a surface composed of relatively small protein subunits in identical local environments. Exact icosahedral point symmetry allowed only 60 subunits (as is the case for STNV) in the shell; however, they proposed that this 'subunit' could itself be composed of several identical subunits which would be packed in 'quasi-equivalent' environments. The theory has been repeatedly confirmed by electron microscopic and X-ray diffraction studies on small viruses and their crystals (*e.g.* Klug, Longley & Leberman, 1966).

An attempt is being made to solve the structure of STNV at high resolution by either the isomorphous replacement (Green, Ingram & Perutz, 1956) or molecular replacement methods (Rossmann & Blow, 1963). The former involves the preparation of isomorphous heavy-atom derivatives of the virus and the determination of the positions of those heavy atoms in the crystal. Heavy atoms attached specifically to the coat protein would have the same symmetry as the protein shell and that high symmetry would then facilitate a solution for the positions by either, (1) a brute-force trial-and-error search of the 'asymmetric volume' of the protein coat region, testing each possible position by generating the symmetry-related set and comparing calculated structure factors for the set with the observed $|\Delta F|$ set for a specific trial derivative, or (2) comparison of the observed heavy-atom difference Patterson function with a calculated vector set (Nordman & Nakatsu, 1963), again by a systematic search of the 'asymmetric volume' of the protein region and generation of the particle symmetry related set to use to generate the vector set. The molecular replacement method depends on real or reciprocal-space averaging to generate or improve phases when the crystallographic asymmetric unit possesses a known point symmetry. Both methods depend very much on a precise knowledge of the locations of the symmetry axes.

The non-crystallographic symmetry in X-ray diffraction patterns from virus crystals has been analyzed by two approaches; inspection of the direct or weighted X-ray diffraction pattern (Caspar, 1956) and analysis by superposition methods of the Patterson function obtained from the diffraction data (Åkervall *et al.*, 1971,pp. 469–483). Analysis of virus symmetry by direct inspection of precession films is facilitated when a number of the virus particle symmetry axes are situated within a few degrees of the observed reciprocal-lattice plane. The symmetry is manifested in a series of 'spikes' of intense reflexions radiating from the lattice origin. The angular relations between those spikes allow assignment of the symmetry of each spike and the orientation of the particle with respect to the crystal axes. Although the method is most easily applied when, as is the usual case for the small spherical viruses, the particle lies on a special position in the lattice such that one or more of the particle symmetry axes are incorporated in the crystal symmetry, it has also been successfully applied to crystals of broad bean mottle virus (Finch, Leberman & Berger, 1967) where there are two complete particles per asymmetric unit.

The second method, analysis of the Patterson function by means of the rotation function (RF; Rossmann & Blow, 1962) was used for the STNV study. The RF has been used with many protein crystal data sets to locate non-crystallographic symmetry axes within a crystallographic asymmetric unit, for example, the non-crystallographic dyads in rhombohedral insulin crystals (Dodson, Harding, Hodgkin & Rossmann, 1966) and in monoclinic $\alpha$-chymotrypsin (Blow, Rossmann & Jeffrey, 1964) crystals, both of which were subsequently confirmed by the high-resolution structure determinations.

However, when the RF was calculated with 15 Å three-dimensional STNV data (Åkervall *et al.*, 1971, pp. 469–483) the rather large number of poorly resolved peaks and the dominance of the calculation by extra peaks resulted in a misinterpretation in favour of octahedral symmetry. The results were subsequently reinterpreted (Klug, 1971; Åkervall *et al.*, 1971, pp. 487–488) as being consistent with icosahedral particle symmetry.

The purposes of the study reported here were, (1) to determine conditions for calculating the RF with better peak resolution and, (2) to refine the particle orientation to obtain sufficient precision to use for interpreting heavy-atom difference Patterson functions and/or for symmetry averaging electron density maps.

## Experimental

The virus crystals were grown on a small plateau in a thin-walled glass capillary by feeding concentrated virus solution to a small seed crystal placed on the plateau (Åkervall & Strandberg, 1971). When the crystals had grown to be wedged into the capillary, they were drained and the ends of the capillary sealed with wax with the usual precaution of leaving some mother liquor in the tube to maintain vapor pressure. The crystals were plates generally 0·25 mm thick and 1·5 mm long wedged in 1·0–1·5 mm diameter capillaries. The 10 Å data set consisted of 29 single-layer, $\mu=5°$ precession-film sets taken with a Buerger–Supper precession camera at a crystal-to-film distance of 100 mm. The X-ray source was an Elliott GX6 rotating anode tube operated at 2·8 kW giving a 0·2 mm square viewed source. A copper anode and a nickel-foil filter were used. The intensities were measured with an automatic analogue-integrating microdensitometer constructed by Dr V. Klimecki of the Chemistry Department, University of Uppsala, Sweden. The data set was 90% complete to 12 Å resolution and 70% complete to 10 Å; reflexions beyond 10 Å were excluded from all calculations. No correction was made for absorption. A collimator with a 0·25 mm circular aperture was used for most films although some layers required a 0·15 mm aperture collimator to ensure spot separation.

No correction was made for differences in scattering volume for different reflexions on the same layer owing to the precession of the crystal in a beam smaller than the crystal. Calculations indicated that the maximum volume change was 10% for any one layer at $\mu=5°$.

### The rotation function

The rotation function is a product function of two Patterson functions with superposed origins; one is held stationary and the other rotated about the three angles necessary to acheive any general orientation. The Patterson functions are the same when looking for non-crystallographic symmetry within an asymmetric unit or from different data sets when looking for the angular relationship between different asymmetric units. For computational purposes the RF may be expressed as

$$R(\kappa,\psi,\varphi)=\sum_{p}|F_p|^2\Big(\sum_{h}|F_h|^2\,G_{hp}\Big)$$

where $R(\kappa,\psi,\varphi)$ is the value of the function when the two Patterson functions are related by a rotation matrix [C] defined by the angles $\kappa,\psi,\varphi$ and $G_{hp}$ is a diffraction function dependent on the volume around the origin to be searched (the 'radius of integration') and on the argument

$$\mathbf{H}=(\mathbf{h}+[\tilde{\mathrm{C}}]\mathbf{p})\,.$$

As $\mathbf{H}$ goes to zero, $G_{hp}$ goes to one; as $\mathbf{H}$ goes to infinity, $G_{hp}$ goes to zero.

To observe the symmetry elements within a virus particle and to minimize the effects from cross-vector between particles, the maximum length of the vectors incorporated in the calculation is generally somewhat less than the anticipated diameter of the asymmetric unit. In most reports on the use of the RF the data used, suitably modified to remove the origin, extends from the origin or a rather low cut-off angle (frequently not specified) out to some intermediate resolution, often 4 to 6 Å, which is usually adequate to

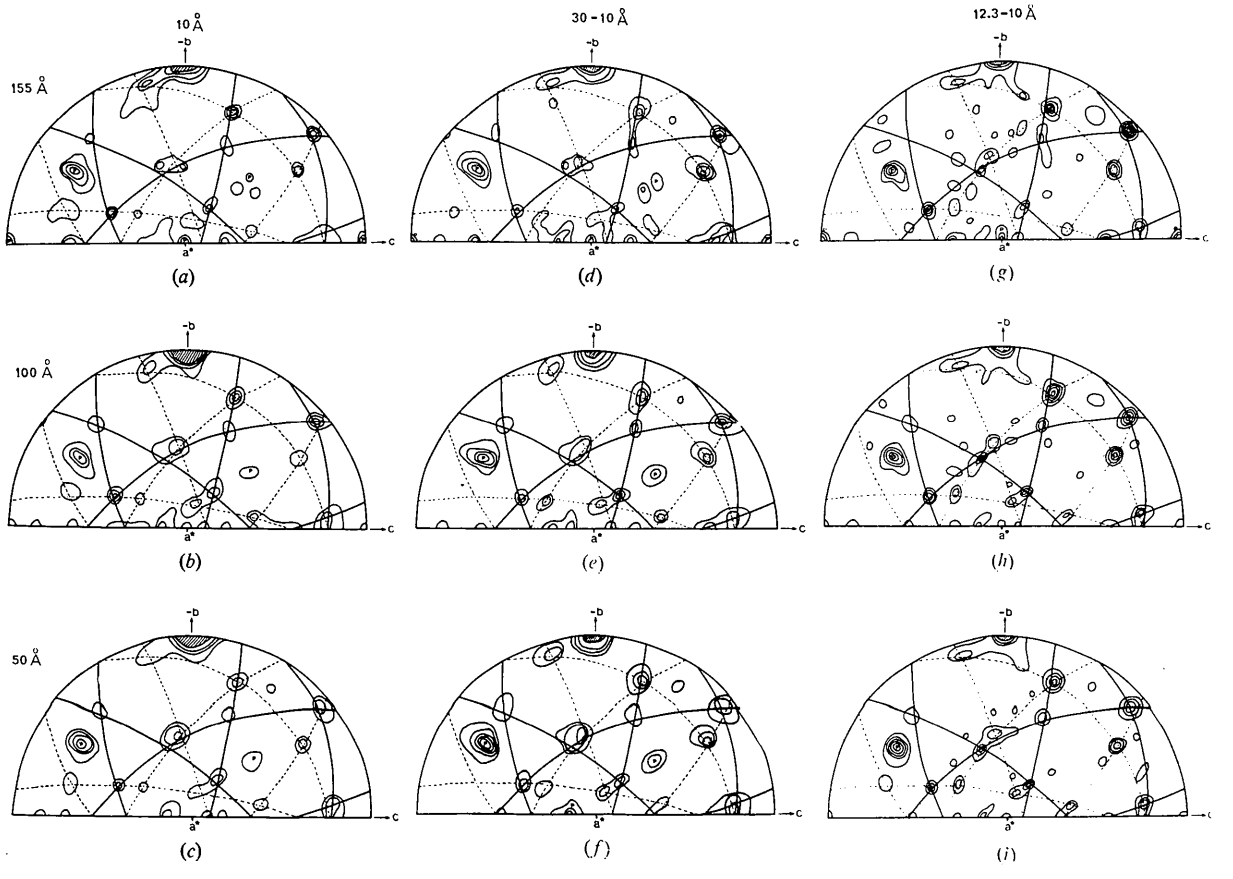


Fig. 1. STNV rotation function sections of constant $\kappa=180°$. (*a*) to (*c*) All data to 10 Å resolution, 476 terms in the large-term Patterson function; radii of integration, (*a*) 155 Å, (*b*) 100 Å, (*c*) 50 Å. (*d*) to (*f*) Data between 30 and 10 Å, 575 terms in the large-term Patterson function; radii of integration, (*d*) 155 Å, (*e*) 100 Å, (*f*) 50 Å, (*g*) to (*i*) Data between 12·3 and 10 Å, 477 terms in the large-term Patterson function; radii of integration, (*g*) 155 Å, (*h*) 100 Å, (*i*) 50 Å. In this and subsequent $\kappa=180°$ sections, the symmetry axes are located at the intersection of *like*-coloured great circles. Continuous lines refer to great circles joining twofold axes of the front surface of one icosahedron; dashed lines, to those on the front surface of the crystallographically related icosahedron.

resolve unambiguously the peak maxima. To minimize computation time only a fraction, frequently about 10%, of the largest reflexions in several resolution shells is used for calculating the rotated ('large term') Patterson function; the other includes all the data.

### Sources of the peaks in the STNV rotation function

There are three attributable types of non-origin peaks in the RF from STNV data; those due to non-crystallographic symmetry elements of each individual particle in the cell, those due to non-crystallographic symmetry elements relating the self-vector sets of the individual particles, and those due to packing of the particles into the $C2$ crystal lattice which at very low resolution (*ca.* 40 Å) is pseudo-face-centred, '$F222$'. The heights and to some extent the locations of the peak maxima of all three types are affected by both the resolution of the data included and by the integration radius of the individual RF calculation.

### Choice of parameters for the rotation function calculation

Åkervall *et al.* (1971) had observed a significant improvement in the resolution of the RF when they simultaneously reduced the radius of integration, included data to a somewhat higher resolution, and excluded very low resolution data. However, they did not report the effects of these measures taken separately. A series of constant $\kappa$ rotation function sections were calculated to study the effect of each of the parameters.

(1) *The effect of the integration radius*

A series of $\kappa=180°$ sections calculated with 155, 100, and 50 Å integration radii for each of three resolution limits is shown in Fig. 1. The arcs are great circles connecting particle twofold axes and indicate the best fit discussed later. At all three limits the reduction of the integration radius causes some improvement in the apparent peak resolution, although the major change is achieved in the step from 155 to 100 Å and a further decrease has less effect. The result of reducing the radius is a qualitative decrease in the overall background level rather than an improvement in resolution or a change in the relative peak heights.

The radius of the STNV particle is known to be about 85 Å from electron microscopic studies (Fridborg *et al.*, 1965). Thus, in the earlier STNV study an integration radius of 155 Å was used, expecting thereby to limit the calculation primarily to intraparticle vectors. In retrospect it is apparent that such a radius includes a large number of cross-vectors and

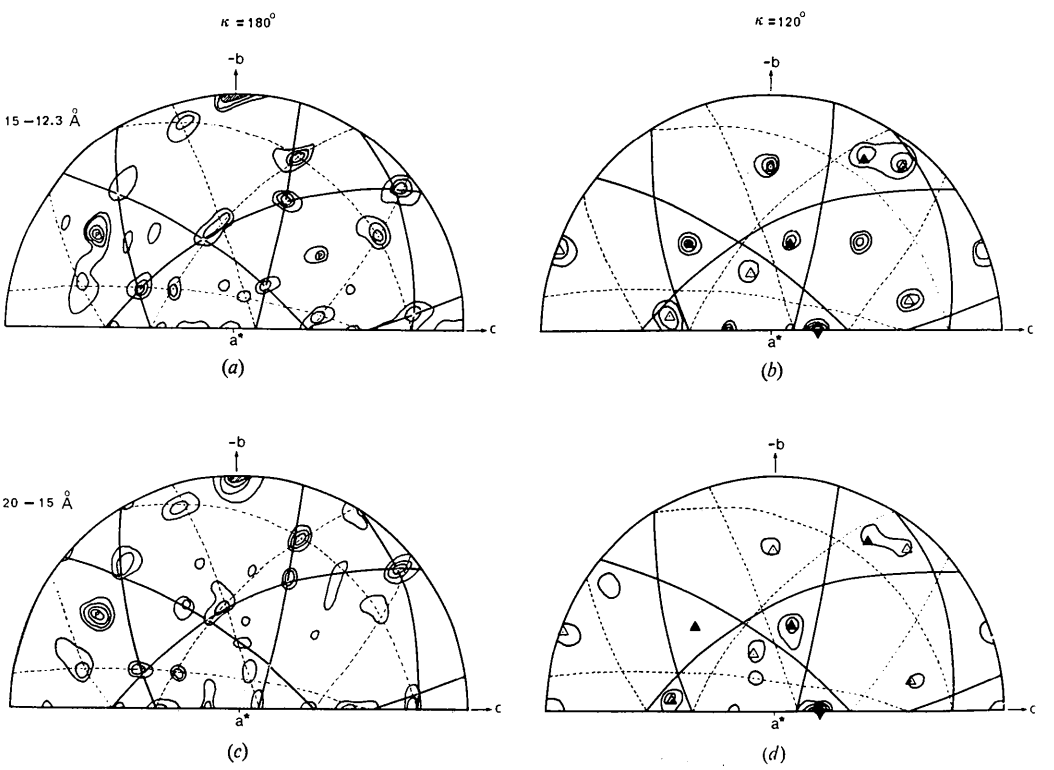


Fig. 2. STNV rotation function sections for thin shells of intermediate resolution data. (*a*) and (*b*) Data between 15 and 12·3 Å resolution, 268 terms in the large-term Patterson function, 50 Å radius of integration. (*a*) $\kappa=180°$, (*b*) $\kappa=120°$. (*c*) and (*d*) Data between 20 and 15 Å resolution, 196 terms in the large-term Patterson function, 50 Å radius of integration. (*c*) $\kappa=180°$, (*d*) $\kappa=120°$.

that the integration radius must be decreased to somewhat closer to the subunit diameter (30 to 60 Å) to limit the calculation to *intersubunit* vectors. The desired symmetry is that of the set of subunits forming the viral outer shell rather than that of the entire particle. The overall particle symmetry in the crystal depends on the degree to which the viral ribonucleic acid is ordered. We have not yet been able to detect to what degree, if any, the nucleic acid is ordered, however, if it were ordered and packed asymmetrically in the virus, it might well be one source of the 'noise' in the 155 Å radius calculation.

(2) *The effect of the data resolution limits*

Figs. 1 and 2 show a series of sections calculated with a 50 Å radius of integration radius and a variety of upper and lower limits on the resolution of data included. The most obvious effects of varying the limits are that removing the very low angle reflexions eliminates the pseudo-origin peaks at $\psi=90°$, $\varphi=0°$ and 90° (=270°) and that the addition of higher-angle reflexions leads to increasingly better resolution between adjacent particle symmetry peaks provided that the inner terms are also eliminated. At the extreme where only the 12·3 to 10 Å reflexions were used, all particle peaks in the $\kappa=180°$ section are resolved. Sharpening of the RF by removing the low resolution data was suggested by Rossmann & Blow in the original paper on the method (Rossmann & Blow, 1962). It is analogous to looking at the distribution of the strong reflexions in the highest resolution shell of diffraction data to see if the 'spikes' and thus, the particle symmetry, persist to the resolution limit.

All the RF calculations were initially done at 5° intervals in $\psi$ and $\varphi$. However, as higher resolution data was added, the peaks became so compact as to fall between the grid interval, and the observed peak heights were a function of the distance of the nearest grid point from the true peak maximum rather than of the amount of overlap between the Patterson functions. Additional grid points at 1° intervals were calculated around each of the particle symmetry-axis locations to establish the peak locations and heights. The three sections in Fig. 3 have been augmented with the extra points. In estimated standard deviations above the mean, the mean particle symmetry peak height for non-overlapped peaks was 3·6, the minimum was 2·8 and the maximum was 4·6. There was no obvious correlation of peak height with the symmetry type of the axis.

## Numerical fit of an icosahedron to the STNV rotation function

To obtain the best fit of an icosahedral symmetry axis set to the RF and to estimate the precision of that fit a computer program was written which compared the location of the known peak maxima with the location of a model set of symmetry axes rotated through an Eulerian angle set. The model axes set consisted of the direction cosines of the symmetry axes of an icosahedron which were determined by simple geometry (*cf. International Tables for X-ray Crystallography,* 1967). Two criteria of fit were calculated. The first was the absolute spherical angular separation, $\delta$, between the model axes and the observed peak maxima. The angle is given by Rossmann, Ford, Watson & Banaszak (1972) as,

$$\cos\delta=\sin\psi_{obs}\sin\psi_{calc}\cos(\varphi_{obs}-\varphi_{calc})+\cos\psi_{obs}\cos\psi_{calc}\,.$$

The best fit was taken to be that set of the three Eulerian angles $(\theta_1,\theta_2,\theta_3)$ which gives the lowest root-mean-square angular deviation, r.m.s. $\delta$, which is given by,

$$\text{r.m.s. }\delta=(\sum^{n}\delta^2/n)^{1/2}\,.$$

The sum is over the 31 independent peak locations. The second criterion depended upon the value, $R$, of the RF at the positions of the rotated model axes, that value being generated by linear interpolation using the three nearest points in the calculated grid. The best fit by this criterion was that set of angles which gives the lowest root-mean-square difference between $R$ at

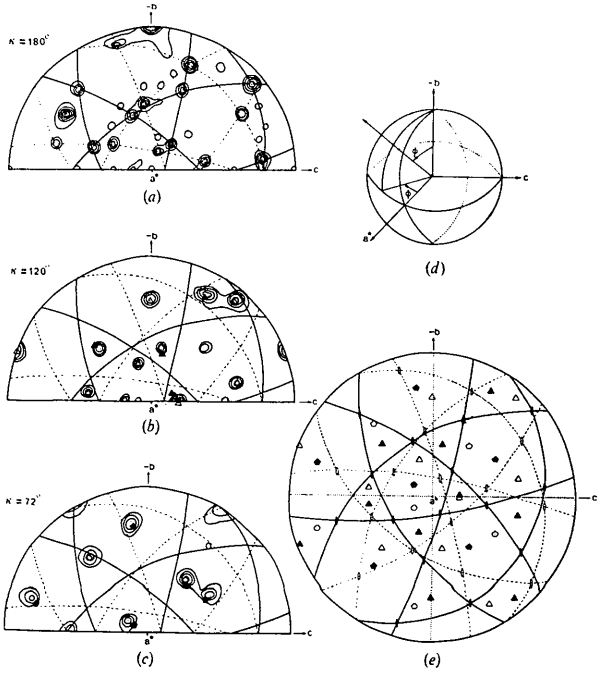


Fig. 3. Augmented rotation function sections for the 12·3 to 10 Å data shell. 477 terms in the large-term Patterson function. 50 Å radius of integration, (*a*) $\kappa=180°$, (*b*) $\kappa=120°$, (*c*) $\kappa=72°$. In (*b*) and (*c*) the filled symmetry elements are displaced so as not to obscure the peaks. (*d*) shows the $\varphi$ and $\psi$ angles in relation to the crystal axial system. (*e*) Stereographic projection down [100] of the front halves of the axial systems of the two icosahedra related by the two fold axis parallel to **b**. The vertical dotted line marks the $\varphi=0°$ line, the horizontal dotted line marks the $\psi=90°$ line.

the model axis locations and $R$ at the calculated peak maxima. The difference is normalized to avoid biasing the heavier peaks. The r.m.s. $\Delta R$ is then

$$\text{r.m.s. } \Delta R = \left[\sum^{n}\left(\frac{\Delta R}{R_{\max n}}\right)^2 / n\right]^{1/2}.$$

This interpretation of the RF in terms of the fit of a known symmetry axis set is very similar to the 'locked rotation function' used by Rossmann *et al.* (1972) on the RF from glyceraldehyde phosphate dehydrogenase crystal data. The main differences are the criteria for evaluating the fit and the thoroughness of the search. Rossmann *et al.* searched the entire $\kappa = 180°$ section to find the best fit to a 222 axis set, while in this study the proper symmetry relationship of the peaks in the RF had been determined previously and it was necessary only to refine the fit.

Beginning with the model axis oriented in the cell such that three of the model twofold axes are parallel to **a***, **b**, and **c** as in Fig. 4(*a*), the orientation angles are: $\theta_1$, rotation about $X_3$, the axis parallel to **c**; $\theta_2$, rotation about the rotated axis $X_1$, which was originally parallel to **a***; $\theta_3$, rotation about the rotated axis $X_3$, which started parallel to **c**. All rotations are clockwise looking down the axes toward the intersection of the axes.

The fit criteria were calculated for a three-dimensional grid with an interval of 0·1° along each grid direction. Fig. 5 shows two intersecting planes through what was found to be the best fit, on the basis of a minimum r.m.s. $\delta$, for each of the two criteria. The r.m.s. $\delta$ gave a single minimum of 0·67° at $\theta_1 = -70{\cdot}3$, $\theta_2 = -14{\cdot}4$, $\theta_3 = 22{\cdot}0°$. The largest deviation was 1·4°. The single minimum in r.m.s. $\Delta R$ was at $\theta_1 = -70{\cdot}3$, $\theta_2 = -14{\cdot}5$, $\theta_3 = 22{\cdot}0°$. As the r.m.s. $\delta$ was less than the sampling interval and therefore the fit might be limited by the RF grid interval rather than the inherent angular error, the calculation was repeated with an RF grid calculated at 0·5° intervals and the orientation angles scanned in 0·05° intervals. The best point was found at $\theta_1 = -70{\cdot}30$, $\theta_2 = -14{\cdot}35$, $\theta_3 = 22{\cdot}00°$, r.m.s. $\delta = 0{\cdot}67°$. The lack of change suggests that we have the best fit possible at this resolution.

Fig. 4 shows 85 Å radius icosahedra in the STNV lattice, (*a*) in the standard orientation before rotation, (*b*) rotated to the best fit angles obtained above, (*c*) a diagram of several cells with the icosahedra positioned (Rossmann, Åkervall, Lentz & Strandberg, 1973) and oriented properly.

### Error in symmetry-related positions

If a point at $x$ is rotated by a particle twofold axis to a point $x'$ and the angular error in the axis location is $\delta$, then the angular error between $x'$ and the point $x''$ to which $x$ would be rotated by the 'correct' axis position is $2\delta$. Using the particle symmetry-axis locations from the best fit to generate symmetry-related sites in the virus, then a $\delta$ of 0·67° would result in an error of 1·3° in related positions. At a radius of 85 Å this corresponds to an error of 1·9 Å. As that is less than one fifth the resolution at 10 Å, we believe that the axes are located with sufficient precision for the above-mentioned calculations.

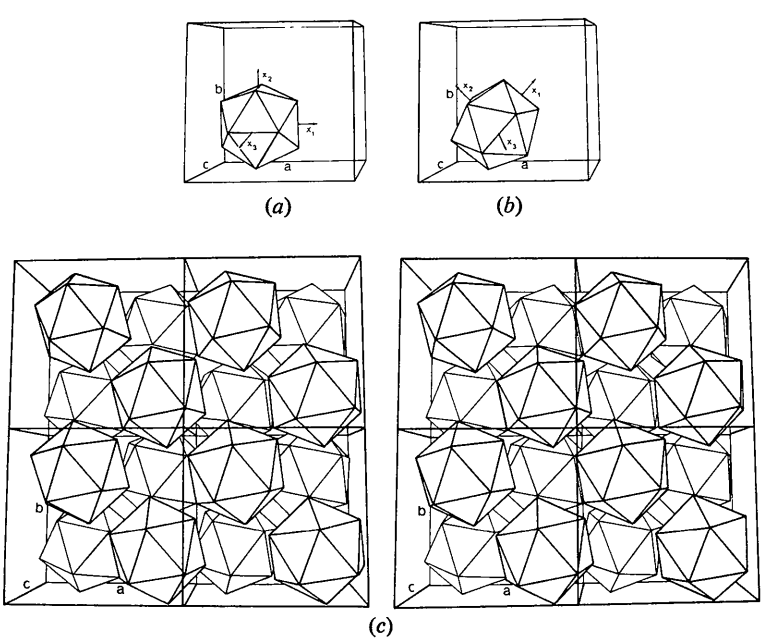


Fig. 4. *ORTEP* (Johnson, 1965) drawings of icosahedra in the crystal lattice (*a*) before rotation, (*b*) after rotation to the best fit angles, (*c*) Packing diagram of 85 Å radius (centre to vertex), icosahedra properly oriented and positioned in the crystal lattice. As the $\beta$ angle is 94·6° in this cell, **a*** is very nearly parallel to **a** and it was not included in the diagram. $x_1$ in (*a*) is parallel to **a***.

### The extra peaks in the STNV rotation function

Although there is no general theory for the prediction of extra symmetry peaks in the RF (Rossmann, 1973), this and earlier studies on STNV indicate some likely sources of those peaks. We have observed, (1) packing peaks caused by the dominance of the RF by very low order reflexions which show additional pseudo-symmetry and, (2) extra non-crystallographic symmetry accompanied by overlapping non-crystallographic peaks from particles related by a crystallographic axis. Examples of the first type have been mentioned earlier as being due to the pseudo-$F222$ symmetry of the reflexions with spacings greater than 40 Å. Extra 'origin' peaks are generated at $\psi=90°$, $\varphi=0$ and 90°. In the STNV RF they are eliminated by excluding reflexions with spacing greater than 30 Å. Extra peaks of the second type occur when the RF calculation is dominated by reflexions from spacings too coarse to resolve nearby particle non-crystallographic symmetry peaks. This may be due either to the inclusion of too much lower resolution data or to the lack of higher resolution terms. Using the 30 to 12·3 Å data a number of extra and overlapped peaks

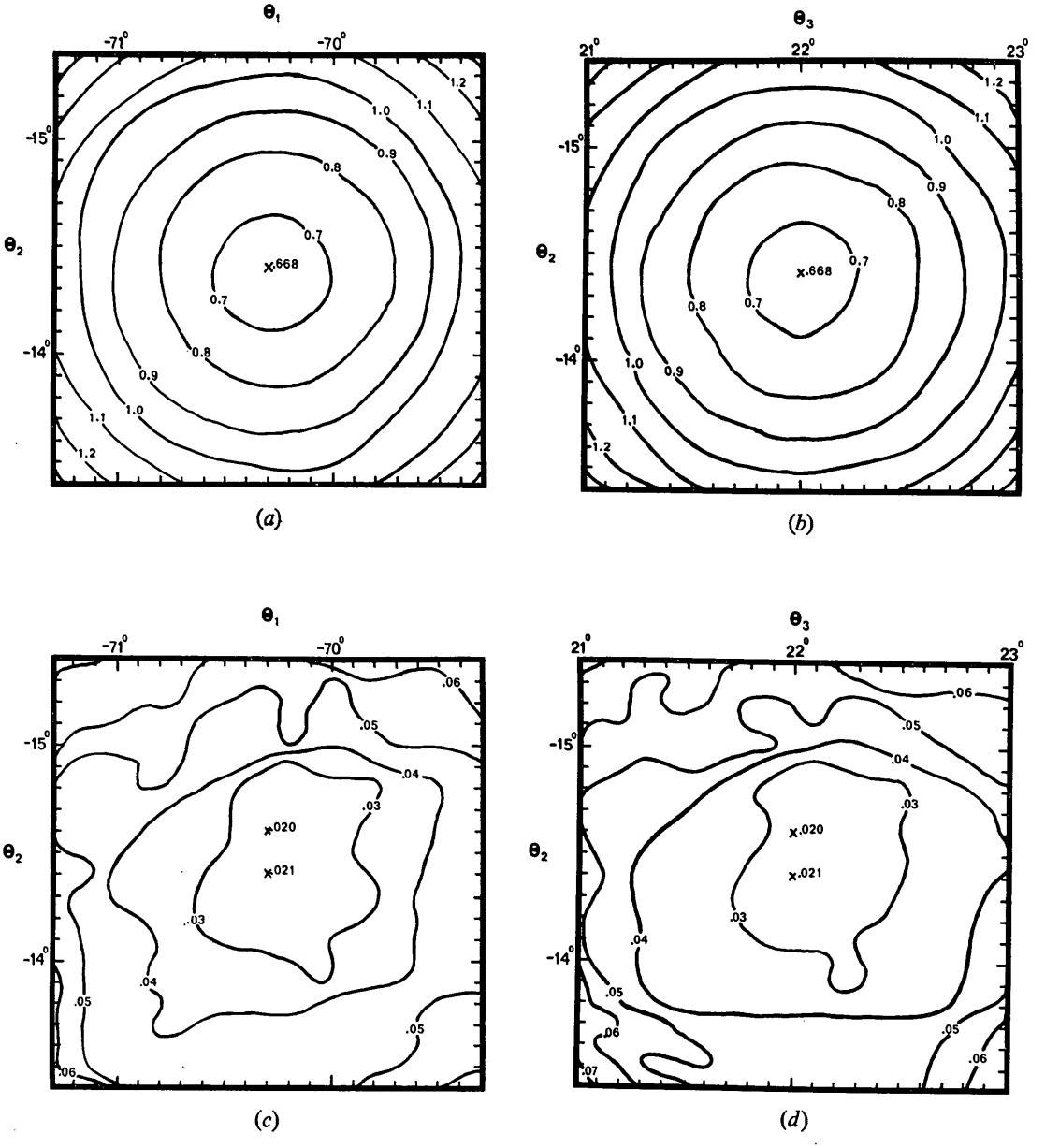


Fig. 5. Sections through the minima in the three-dimensional plots of the two fit criteria defined in the text. (*a*) and (*b*) are, respectively, constant $\theta_3$ and $\theta_1$ sections through the plot of r.m.s. $\delta$. (*c*) and (*d*) are constant $\theta_3$ and $\theta_1$ sections through the plot of r.m.s. $\Delta R$.

occur only because of the inclusion of the lower resolution terms (Åkervall *et al.*, 1971, pp. 487-488). Using only the 15 to 12·3 Å shell, Fig. 2(*a*) and 2(*b*), all particle peaks are resolved except the threefold axes at $\psi=90°$, $\varphi=158°$ (=338°). Even the 20 to 15 Å shell, Fig. 2(*c*) and 2(*d*), is sufficient to resolve one of the threefold axis overlaps which had been present with the 30 to 12·3 Å data. With the 12·3 to 10 Å data all particle peaks are well resolved exept the threefold axes at $\psi=90°$, $\varphi=158°$. This lack of resolution of the threefold axes means that on the line perpendicular to those axes, that is, $\varphi=68°$ (=248°), and at an angle of 120° from **b** or $-$**b**, that is $\psi=60$ and 120°, there is apparent two fold symmetry near the origin in the Patterson function and, thus, an extra symmetry peak on the $\kappa=180°$ section. Recalculation of the numerical fit as above without the overlapped threefold-axis peak showed that those axes are within 0·6° of superposition at the best fit angles.

## Conclusions

The rotation function of STNV can be readily interpreted even with rather low resolution data providing conditions are chosen which emphasize the intersubunit vectors and minimize the lattice packing effects. With STNV data this was achieved by decreasing the integration radius and working with a thin shell of the highest resolution data available. Requiring the simultaneous fit of a large number of compact, well resolved peaks results in a high precision in the orientation angles. The low r.m.s. angular deviation indicates that the particle symmetry does not deviate from icosahedral at this resolution.

We are grateful to Professor Michael G. Rossmann and Dr K.K. Kannan for many fruitful discussions and helpful suggestions. We thank Mrs G. Johansson for typing the manucript. This work has been supported by grants from the Faculty of Science, University of Uppsala, the Swedish Computing Authorities (Statskontoret, Stockholm), the Swedish Medical and Natural Science Research Councils, the Tricentennial Fund of the Bank of Sweden and the Knut and Alice Wallenberg Foundation. We are particularly grateful for the helpful cooperation of Drs W. Schneider, H. Sundberg and A. Öst and the rest of the staff at the Uppsala University Data Center. During part of this work one of us (PJL) was the recipient of an NIH postdoctoral fellowship.

## References

Åkervall, K. & Strandberg, B. (1971). *J. Mol. Biol.* **62**, 625–627.

Åkervall, K., Strandberg, B., Rossmann, M. G., Bengtsson, U., Fridborg, K., Johannison, H., Kannan, K., Lövgren, S., Petef, G., Öberg, B., Eaker, D., Hjerten, S., Ryden, L. & Moring, I. (1971). *Cold Spring Harbor Symp. Quant. Biol.* **36**, 469–483, 487–488.

Blow, D. M., Rossmann, M. G. & Jeffrey, B. A. (1964). *J. Mol. Biol.* **8**, 65–78.

Caspar, D. L. D. (1956). *Nature, Lond.* **177**, 475–476.

Caspar, D. L. D. & Klug, A. (1962). *Cold Spring Harbor Symp. Quant. Biol.* **27**, 1–24.

Crick, F. H. C. & Watson, J. D. (1956). *Nature, Lond.* **177**, 473–475.

Crowfoot, D. & Schmidt, G. M. J. (1945). *Nature, Lond.* **155**, 504–505.

Dodson, E., Harding, M. M., Hodgkin, D. C. & Rossmann, M. G. (1966). *J. Mol. Biol.* **16**, 227–241.

Finch, J. T., Leberman, R. & Berger, J. E. (1967). *J. Mol. Biol.* **27**, 17–24.

Fridborg, K., Hjerten, S., Höglund, S., Liljas, A., Lundberg, B. K. S., Oxelfelt, P., Philipson, L. & Strandberg, B. (1965). *Proc. Natl. Acad. Sci. U.S.* **54**, 513–521.

Green, D. W., Ingram, V. M. & Perutz, M. F. (1954). *Proc. Roy. Soc.* A**225**, 287–307.

*International Tables for X-ray Crystallography* (1967). Vol. II, 2nd ed., pp. 46–49. Birmingham: Kynoch Press.

Johnson, C. K. (1965). *ORTEP: A Fortran Thermal-Ellipsoid Plot Program for Crystal-Structure Illustrations.* Report ORNL-3794, Oak Ridge National Laboratory, Oak Ridge, Tennessee.

Kassanis, B. & Nixon, H. L. (1961). *J. Gen. Microbiol.* **25**, 459–471.

Klug, A. (1971). *Cold Spring Harbor Symp. Quant. Biol.* **36**, 483–487.

Klug, A., Longley, W. & Leberman, R. (1966). *J. Mol. Biol.* **15**, 315–343.

Nordman, C. E. & Nakatsu, K. (1963). *J. Amer. Chem. Soc.* **85**, 353.

Rossmann, M. G. (1973). *Trans. Amer. Cryst. Assoc.* **9**, 101–122.

Rossmann, M. G., Åkervall, K., Lentz, P. J. Jr & Strandberg, B. (1973). *J. Mol. Biol.* **79**, 197–204.

Rossmann, M. G. & Blow, D. M. (1962). *Acta Cryst.* **15**, 24–31.

Rossmann, M. G. & Blow, D. M. (1963). *Acta Cryst.* **16**, 39–45.

Rossmann, M. G., Ford, G. C., Watson, H. C. & Banaszak, L. J. (1972). *J. Mol. Biol.* **64**, 237–249.

Stanley, W. M. (1935). *Science*, **81**, 644.